Understanding Galaxy Morphology Evolution Through Cosmic Time via Redshift Conditioned Diffusion Models

Andrew Lizarraga[1], **Eric Hanchen Jiang**[1], **Jacob Nowack**[2],
Yun Qi Li[3], **Ying Nian Wu**[1], **Bernie Boscoe**[2], **Tuan Do**[4]

[1]Department of Statistics and Data Science, UCLA
[2]Department of Computer Science, Southern Oregon University
[3]Department of Physics and Astronomy, University of Washington
[4]Department of Physics and Astronomy, UCLA

{andrewlizarraga, ericjiang0318, yunqil}@g.ucla.edu,
{boscoeb, nowackj}@sou.edu , ywu@stat.ucla.edu, tdo@astro.ucla.edu
https://github.com/astrodatalab/lizarraga_2024

Abstract

Redshift measures the distance to galaxies and underlies our understanding of the origin of the Universe and galaxy evolution. Spectroscopic redshift is the gold-standard method for measuring redshift, but it requires about 1000 times more telescope time than broad-band imaging. That extra cost limits sky coverage and sample size and puts large spectroscopic surveys out of reach. Photometric redshift methods rely on imaging in multiple color filters and template fitting, yet they ignore the wealth of information carried by galaxy shape and structure. We demonstrate that a diffusion model conditioned on continuous redshift learns this missing joint structure, reproduces known morphology-z correlations. We verify on the HyperSuprime-Cam survey, that the model captures redshift-dependent trends in ellipticity, semi-major axis, Sérsic index, and isophotal area that these generated images correlate closely with true redshifts on test data. To our knowledge this is the first study to establish a direct link between galaxy morphology and redshift. Our approach offers a simple and effective path to redshift estimation from imaging data and will help unlock the full potential of upcoming wide-field surveys.

1 Introduction

Understanding the intricate processes of galaxy formation and evolution represents a frontier challenge in modern astrophysics. Galaxies are not static entities but dynamic systems that undergo profound transformations in morphology, structure, and composition over cosmic times. Fundamental to these studies, redshift (denoted z) is an indispensable observational measurement for cosmic time and distance, enabling the study of galaxies at different evolutionary stages. However, the inability to continuously observe individual galaxies throughout their multi-billion-year lifespans imposes a fundamental limitation, restricting empirical studies to statistical ensembles from discrete temporal snapshots, e.g. using redshift. Additionally, unlike photometric surveys such as the Sloan Digital Sky Survey (SDSS) Ahn et al. [2012], the Dark Energy Survey (DES) Abbott et al. [2022], the Kilo-Degree Survey (KiDS) Kuijken et al. [2019], and the Hyper Suprime-Cam (HSC) Survey Aihara et al. [2019], comprised of potentially millions or billions of galaxies, redshift-matched surveys, such as Do et al. [2024a] often comprise of a few 100,000 samples due to the computational time, cost, and effort of computing the redshift. To the author's knowldedge there is still no reliable

Preprint. Under review.

method for predicting redshift given photometric images due to concerns of deep learning models not learning to utilize physical properties of galaxy structure in order to make a prediction. Here, we investigate the potential of generative models, conditioned on redshift, to bridge this observational chasm by synthesizing high-fidelity galaxy populations across cosmic time, thereby offering a novel computational lens for simulating and understanding their evolutionary trajectories [Nguyen et al., 2024, Lastufka et al., 2024].

Among emerging generative techniques, Denoising Diffusion Probabilistic Models (DDPMs) have demonstrated exceptional capabilities in producing highly realistic imagery across diverse scientific and visual domains [Sohl-Dickstein et al., 2015a, Ho et al., 2020a, Nichol and Dhariwal, 2021, Dhariwal and Nichol, 2021, Zhu et al., 2024], and their application to astrophysical data is beginning to show considerable promise [Li et al., 2024b, Xue et al., 2023, Smith et al., 2022, Lizarraga et al., 2024a, Jiang et al., 2024]. A critical unresolved challenge, however, lies in effectively conditioning these models on continuous physical parameters intrinsic to astrophysical systems, such as redshift. While there have been appoaches using continuous conditioning for DDPM's such as Ding et al. [2024], or Sohl-Dickstein et al. [2015b], current prevalent approaches for galaxy modeling resort to parameter discretization inevitably sacrifice information and fail to capture the continuous nature of galaxy evolution Li et al. [2024b].

In this study, we develop and evaluate a DDPM framework conditioned directly on continuous redshift values. We aim to demonstrate two principal advances: First, the capacity of such models to learn the conditional distribution $p(X|z)$ of galaxy images X given any redshift z, thereby implicitly encoding the redshift-dependence of morphological characteristics. Second, we explore the model's ability under to generate galaxies conditioned at different cosmic time-points by evaluating physical metrics of the images produced. We find that the model correctly captures associated physical structure of galaxies at different time points, purely based on photometry and absent of information about these physical properties of galaxy formation, suggesting that such generative models can in fact produce realistic galaxies that are physically accurate to galaxies at that point in cosmic time.

As a brief review, DDPMs operate via a forward noising process and a learned reverse denoising process Ho et al. [2020b]. The forward process gradually adds Gaussian noise $\epsilon \sim \mathcal{N}(0, I)$ to the data X_0 over T timesteps:

$$q(X_t|X_{t-1}) = \mathcal{N}(X_t; \sqrt{1-\beta_t}X_{t-1}, \beta_t I) \implies X_t = \sqrt{\bar{\alpha}_t}X_0 + \sqrt{1-\bar{\alpha}_t}\epsilon, \tag{1}$$

where β_t are predefined noise variances, $\alpha_t = 1 - \beta_t$, and $\bar{\alpha}_t = \prod_{s=1}^{t} \alpha_s$. The model learns to reverse this process by predicting the added noise $\epsilon_\theta(X_t, t, z)$ given the noisy image X_t, timestep t, and a condition z (the redshift). Generation involves iteratively sampling from $p_\theta(X_{t-1}|X_t, z)$:

$$x_{t-1} = \frac{1}{\sqrt{\alpha_t}} \left(x_t - \frac{\beta_t}{\sqrt{1-\bar{\alpha}_t}} \epsilon_\theta(X_t, t, z) \right) + \sigma_t \mathbf{z}', \quad \mathbf{z}' \sim \mathcal{N}(0, I). \tag{2}$$

We focus on integrating continuous redshift z as a conditioning parameter within the DDPM architecture, and leveraging the learned denoising function $\epsilon_\theta(x_t, t, z)$ to synthesize smooth morphological transitions. While Variational Autoencoders (VAEs) [Kingma and Welling, 2014, Esser et al., 2021] and Generative Adversarial Networks (GANs) [Goodfellow et al., 2014] have been explored for conditional generation, DDPMs offer a distinct framework with advantages in image fidelity and training stability. A core principle of our approach is to ensure that small variations in z induce correspondingly subtle and physically coherent changes in the generated galaxy image X_0 conditioned on z (denoted X_0^z, thereby promoting generation stability under conditioning perturbations [Arjovsky et al., 2017]. The physical similarity of generated galaxies is rigorously assessed through quantitative morphological analysis (Section 4), compared to established astrophysical observations [Conselice, 2014b]. Furthermore, we empirically validate the adherence of our trajectory synthesis methodology to theoretical smoothness assumptions (Section 4). Note that redshift values near 0 represent relatively small cosmological distances and small changes in lookback time. Where redshifts closer to 4 correspond to much larger comoving distances. In order to keep the scale linear we require the following transform: $z' = \log(1 + z)$. In this paper when we state the redshift z, we implicitly assume the log transform has been applied unless stated otherwise.

1.1 Related Work

Generative modeling of galaxy populations has primarily employed Generative Adversarial Networks (GANs) conditioned on redshift to simulate visual characteristics Lanusse et al. [2021], Margalef-Bentabol et al. [2020]. However, GANs are susceptible to training instabilities and mode collapse, and evaluations have often lacked rigorous morphological quantification against physical properties. While Denoising Diffusion Probabilistic Models (DDPMs) offer enhanced image quality and stability [Sohl-Dickstein et al., 2015a, Ho et al., 2020a], their application in astrophysics has largely relied on discretizing continuous parameters like redshift [Li et al., 2024b, Smith et al., 2022]. This discretization fundamentally limits the ability to model the continuous nature of galaxy evolution and smooth morphological transitions.

The challenge of continuous conditioning is recognized across machine learning disciplines Ding et al. [2024], but robust solutions for complex astrophysical parameters like redshift, with direct physical interpretation of generated features, remain underdeveloped. Efforts to incorporate physical priors or leverage simulations [Nguyen et al., 2024, Lastufka et al., 2024, Li et al., 2024b] are complementary but distinct from our data-driven approach, where evolutionary trends are learned directly from observational snapshots conditioned on continuous redshift. This limits the scope of the data the model views to limited cosmic depth, i.e. redshift values between 0 and 1.

1.2 Contribution

Our study provides the following contributions to address these limitations and advance the field:

1. We establish an adaption to continuously-conditioned DDPMs, incorporating redshift perturbation during training to ensure smooth generalization across the redshift continuum. This approach overcomes the information loss associated with discretization.
2. We demonstrate empirically that our model implicitly learns key astrophysically relevant morphological parameters (e.g., size, ellipticity, Sérsic index) and their redshift evolution, without explicit supervision from morphological labels, by solely conditioning on images and their continuous redshift values.
3. To our knowledge, this work presents one of the first systematic constructions and evaluations of continuous galaxy evolutionary sequences from observational data using DDPMs, offering a powerful new data-driven paradigm for investigating galaxy evolution.

2 Dataset

To date, it is prohibitively compute and time-expensive to gather redshift data from spectroscopy and pair the data to the associated photometric images. Consequently, this has severely limited the number of available datasets with matched image-redshift pairs. Among all publicly available datasets, only a few offer sufficient depth and size for training machine learning models for redshift estimation. These include the Sloan Digital Sky Survey (SDSS) Ahn et al. [2012], the Dark Energy Survey (DES) Abbott et al. [2022], the Kilo-Degree Survey (KiDS) Kuijken et al. [2019], and the Hyper Suprime-Cam (HSC) Survey Hiroaki Aihara and et al. [2019].

We employ the **Hyper Suprime-Cam Galaxy Dataset** curated by Do et al. Do et al. [2024b], publicly accessible at Zenodo (GalaxiesML: `https://zenodo.org/records/11117528`, CC-BY 4.0). HSC is the deepest of the completed surveys, with high-quality redshift–image pairs. As shown in Figure 2, HSC achieves an r-band depth of ~ 26.5 AB magnitudes and a source density of $\sim 10^5$ galaxies per square degree—an order of magnitude higher than SDSS and DES. Other upcoming surveys like LSST and Euclid are projected to reach similar or greater depths (shown as pink squares), but their data is not yet publicly released. The dataset comprises 286,401 galaxies, each with spectroscopic redshift measurements spanning $z = 0$ to $z = 4$. Redshift indicates a galaxy's distance and the age of the universe when its light was emitted; for example, $z = 1$ corresponds to light emitted approximately 7.8 billion years ago. Each galaxy is represented by a 64×64 pixel image in five optical wavelength bands: g, r, i, z, y. These filters correspond to progressively redder parts of the visible and near-infrared spectrum. For context, g captures green light at ~ 477 nm, while y captures near-infrared light around ~ 1 μm. Due to selection effects in spectroscopic follow-up, the dataset is biased toward lower redshifts, with about 92.8% of galaxies having $z < 1.5$ (corresponding to light emitted within the past ∼9.5 billion years). We follow the training (204,513 images) and testing (40,914 images) split proposed by Li et al. Li et al. [2024a].

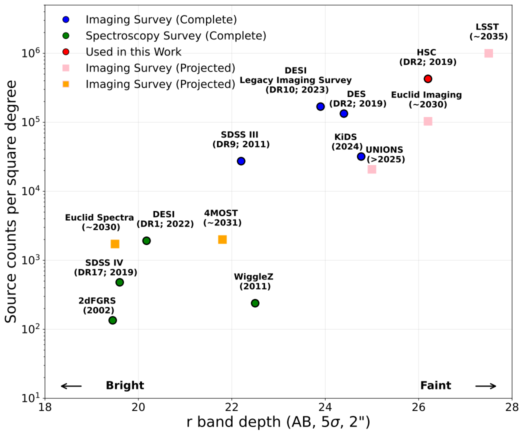

Figure 1: Source density versus r-band depth for major imaging and spectroscopic galaxy surveys. The r-band depth corresponds to the 5σ detection limit in a $2''$ aperture. Each point represents a survey, with completed imaging surveys (e.g., SDSS, DES, KiDS, HSC) shown in solid markers, and projected surveys (e.g., LSST, Euclid) shown in pink outlined squares. The y-axis shows the number of detected sources per square degree on a logarithmic scale. Among publicly available datasets, the Hyper Suprime-Cam (HSC) survey stands out as the deepest complete imaging survey, with a source density of $\sim 10^5$ galaxies per deg^2 and an r-band depth of ~ 26.5 AB magnitudes. These properties make HSC uniquely suited for training deep learning models that require high-resolution, redshift-labeled galaxy images.

3 Methodology

3.1 Continuous Redshift-Conditioned DDPM Architecture

Utilizing DDPMs Ho et al. [2020a], we introduce a novel approach to learn the conditional distribution $p(X^z \mid z)$ by integrating redshift values into the U-Net architecture's time steps Li et al. [2024b], Smith et al. [2022]. To prevent model overfitting and ensure learning is concentrated within a Gaussian neighborhood around specific redshifts z, Gaussian noise $\mathcal{N}(0, \sigma^2)$ is added to the redshifts during training, enhancing the model's ability to interpolate between nearby redshifts. Our Conditional Denoising U-Net starts with a noisy initial galaxy image X_T^z and, through iterative denoising informed by both time step and the adjusted redshifts, aims to produce a clean galaxy image X_0^z. To additionally stabilize the training, we implement an Exponential Moving Average (EMA) Karras et al. [2024] and adhere to a standard variance schedule Ho et al. [2020a], Song et al. [2020] to balance noise addition and preserve data structure.

The model's diffusion process starts with 64×64 pixel galaxies images with 5 channels, which are passed to a noising schedule across $1,000$ time steps, linearly interpolating noise levels from a Beta Start of 1×10^{-4} to a Beta End of 0.02. Training utilizes Huber Loss for its robustness to outliers, gradient clipping with a maximum norm of 1.0, and an AdamW optimizer Loshchilov and Hutter [2020] set to a learning rate of 2×10^{-5}. Redshifts are perturbed with Gaussian noise (std dev 0.01) to prevent overfitting and improve generalization. Our U-Net model, equipped with self-attention layers, varies channels by resolution stage and includes 4 attention heads with layer normalization and GELU activation Hendrycks and Gimpel [2016], applied before and after attention. Temporal and conditional redshift information is encoded using sinusoidal positional encoding of the time step t, transformed into a 256-dimensional vector. This vector is further modified by adding Gaussian noise to the redshift value $z + \mathcal{N}(0, 0.01)$, prior to being fed into the U-Net Fig. 3.1. The model was trained on a single NVIDIA A6000 GPU.

4 Evaluation

Our evaluation aims to quantitatively and qualitatively assess the capacity of our redshift-conditioned DDPM and compare it against recently proposed architectures. The primary objectives were to determine its efficacy in learning meaningful physical and morphological characteristics of galaxies

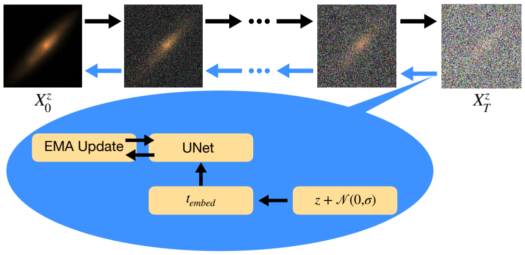

Figure 2: Model Architecture: Our model follows conventional DDPM implementations, but the noise adjust conditioning of z allows the model to better interpolate between it's conditioning for nearby neighborhoods of z.

from image data alone, and its ability to generate physically plausible evolutionary sequences across cosmic time. In particular, we focus on the measured physical attributes of the HyperCam-Suprime survey to gauge the physical consistency of our generated images, which involve five color filters (g, r, i, z, y). While perceptual quality metrics like Fréchet Inception Distance (FID) Heusel et al. [2017] indicate general similarity to true images, they fail to assess critical morphological properties of galaxies and their evolution over time. It's also important to note that the original VGG-Net used in Heusel et al. [2017], was trained on 3-channeled, 256 pixeled RGB images. To compute FID, Li et al. [2024b], Lanusse et al. [2021], propose sub-sampling the color filters to (g, r, i). We follow suit with this in Table 4.1, however we suspect that this is quite a dubious comparison, as we don't compare all the color channels. Moreso, the range of these images is continuous and much larger than that of natural RGB images. To aid our evaluation, we generate synthetic images conditioned on redshifts from the test dataset and compare their physical properties that astronomers typically use to characterize galaxies [e.g. Conselice, 2014a], such as the shape (ellipticity, semi-major axis), size (isophotal area), and brightness distribution (Sérsic index). Furthermore, using the CNNRedshift predictor established by Li et al. Li et al. [2024b], we assess the redshift accuracy against the ground truth, utilizing the redshift loss from Nishizawa et al. [2020]. This redshift predictor was trained on real galaxy images using spectroscopic ground truth and produces good predictions on real data (Fig. 5). These comparisons help verify the physical plausibility of the diffusion model's output. We compute standard morphological metrics for both the test data and the DDPM-generated images conditioned on the test data's redshifts:

- **Ellipticity**: A measure of how elongated a galaxy appears, calculated as $\epsilon = 1 - \frac{b}{a}$, where a and b are the semi-major and semi-minor axes, respectively.
- **Semi-major Axis**: The length of the longest axis of the galaxy's elliptical shape, indicating its size.
- **Sérsic Index**: Describes the intensity profile $I(r)$ of a galaxy as a function of radius r, given by:

$$I(r) = I_0 \exp\left(-b_n\left(\left(\frac{r}{r_e}\right)^{1/n} - 1\right)\right),$$

  where I_0 is the intensity at $r = 0$, r_e is the effective radius, n is the Sérsic index, and b_n is a constant dependent on n. Higher Sérsic indices indicate more concentrated light profiles.
- **Isophotal Area**: The area over which the galaxy emits light above a certain intensity threshold, reflecting the galaxy's apparent size.

Our findings confirm that the DDPM successfully learns the physical characteristics of galaxies even though these attributes were not explicitly provided during training. When comparing the distributions of each metric between the DDPM-generated images and the real data, we observe that the overall shapes of the distributions are very similar, as shown in Figure 3. This indicates that for any conditioned redshift, the model produces physically plausible galaxy images that reflect the morphological diversity present in the real dataset.

In Figure 4, we show that for each redshift bin, the mean values of these metrics for DDPM-generated galaxies closely match those of the real test distribution. The error bars represent the 95% confidence

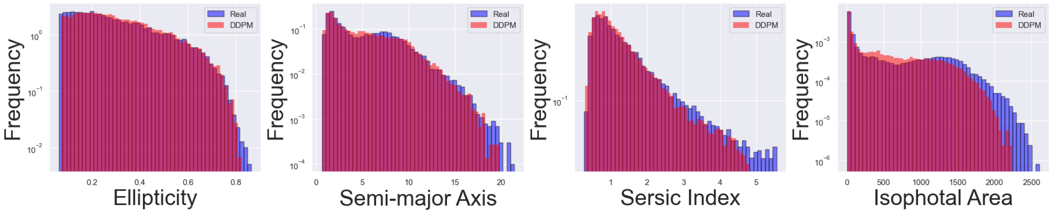

Figure 3: From left to right, the figure displays histograms comparing the frequency distribution of DDPM-generated and real galaxies in terms of 1) ellipticity, 2) semi-major axis, 3) Sérsic index, and 4 isophotal area in the log-scale of redshift z.

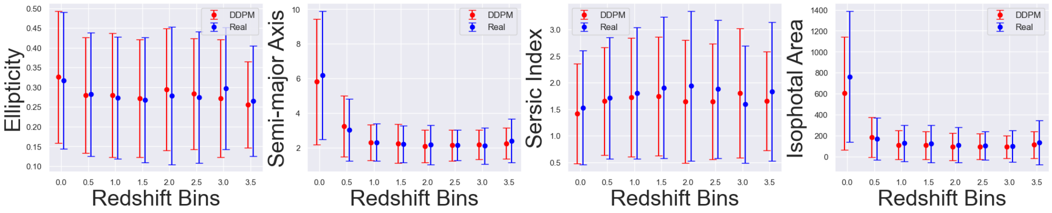

Figure 4: Mean morphological metrics as a function of redshift. Comparison between real test galaxies (orange) and DDPM-generated galaxies (blue) across different redshift bins, with error bars representing 95% confidence intervals on the mean. The model accurately reproduces the observed evolutionary trends in average ellipticity, semi-major axis, Sérsic index, and isophotal area with redshift.

intervals, indicating that the generated images exhibit similar variability to the real data. This suggests that the DDPM model is able to associate redshifts with morphological characteristics of galaxies observed at that redshift, effectively capturing the trends in galaxy evolution.

Although the redshift predictions for generated images show increased variance at higher redshifts (see Figure 5), the morphological characteristics remain physically plausible (Figures 3 and 4). This indicates that while the model captures the general trends in galaxy morphology with redshift, it may produce a broader range of images at higher redshift values, potentially blending characteristics from neighboring redshifts due to data scarcity in those regions. This effect is evident in Figure 6, where the generated images display increased diversity and variability at higher redshifts.

4.1 Benchmarks

There are few generative models trained on deep red-shift survey's (e.g. HyperCam-Suprime). In order to bechmark and compare this model to similar models, we compare against the GAN in Margalef-Bentabol et al. [2020] and the DDPM implemented by Smith et al. [2022]. Since neither of these models were directly using redshift-conditioning, we re-implement these architectures according to their specifications and train continuous red-shift conditioned models using the Guassian perturbation mentioned in Sec. 3 binned, discrete red-shift conditioned versions of the model the performance in terms of FID, Ellipticity, Semi-Major Axis, Sérsic Index, and Isophotal Area can be found in Table 4.1. Additionally, we ablate on σ for the continuous conditioned models and find that our addpation of the DDPM benefits the most from lower values of σ but when $\sigma = 0$ (i.e. discrete conditioning DDPM), the physical measurements take a sharp drop in performance even though the FID is lower. Note we sample $10,000$ redshift values z, from the test set and compute their average Ellipticity, Semi-Major Axis, ect. Then, we take each model synthesize images across all these models and compute the FID (on the false image using the sub-sampling of channels mentioned in earlier), and we compute the average morphological metrics. A lower FID score indicate perceptually similar images, and the other physical metrics are taken as ratios between the average computed in the synthetic data divided by the average computes in the real test data (a score closer to 1 is better). It's worth noting that our model achieve the second best FID score our of the model that were compared, however, our model has notably better performance in terms of the physical benchmarks

Model	FID ↓	Ellipticity %	Semi-Major Axis %	Sérsic Index %	Isophotal Area %
z_{discrete}-cond. GAN Margalef-Bentabol et al. [2020]*	28.7	0.07	0.04	0.61	0.48
z_{discrete}-cond. DDPM Smith et al. [2022]*	**11.6**	0.45	0.22	0.38	0.29
$z_{\text{continuous}}$-cond. GAN $\sigma = 1.0$ Margalef-Bentabol et al. [2020]*	45.0	0.12	0.11	0.68	0.40
$z_{\text{continuous}}$-cond. GAN $\sigma = 0.5$ Margalef-Bentabol et al. [2020]*	30.3	0.11	0.17	0.48	0.39
$z_{\text{continuous}}$-cond. GAN $\sigma = 0.1$ Margalef-Bentabol et al. [2020]*	25.3	0.15	0.20	0.58	0.43
$z_{\text{continuous}}$-cond. DDPM (ours) $\sigma = 1.0$	24.0	0.28	0.50	0.40	0.20
$z_{\text{continuous}}$-cond. DDPM (ours) $\sigma = 0.5$	15.2	0.82	0.70	0.81	0.76
$z_{\text{continuous}}$-cond. DDPM (ours) $\sigma = 0.1$	14.2	**0.98**	**0.96**	**0.93**	**0.90**

Table 1: Quantitative metrics for generative models of galaxy images conditioned on redshift. Lower FID is better; other columns are measured in terms of the proportion of the physical measurements compared to the true galaxy data-test-set measurements (closer to 1 indicates nearly perfect accuracy). Notice that the FID alone is not a good indication if the model is suitable for scientific studies of galaxies. Row 2 has the lowest FID, but the physical measurements of the galaxies produced don't accurately represent physical galaxy characteristics across the redshift values in the test set, despite appearing more realistic.

*Indicates that the original model was not trained on the HyperCam-Suprime survey. We reimplemented and retrained these models with redshift conditioning to keep the comparison as fair as possible.

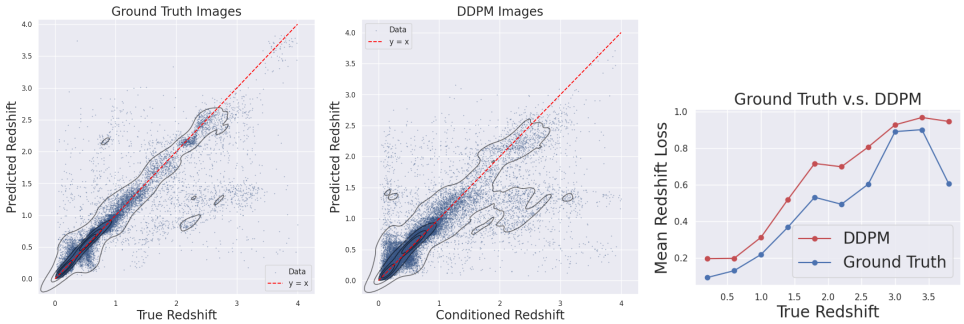

Figure 5: Redshift prediction quality for synthesized galaxies. (Left) CNN-predicted redshift $\hat{z}$ versus true spectroscopic redshift z for real test-set galaxies, demonstrating the baseline accuracy of the independent predictor. (Middle) CNN-predicted $\hat{z}$ versus the input conditioning redshift z for DDPM-generated galaxies, showing strong correlation. (Right) Mean redshift loss, $|\hat{z} - z|/(1 + z)$, as a function of true/conditioned z, confirming good performance in well-sampled regions (e.g., $z < 1.5 - 2.0$) and highlighting increased scatter at higher redshifts due to training data sparsity.

that astronomers typically use. This further supports our hypothesis that conditioning DDPM on redshift is sufficient for the model to implicitly understand some physical properties of galaxies at certain redshift levels. Moreso, being able to appropriately embed the redshift value has a dramatic effect on the model ability to capture physical properties.

4.2 Visual Comparisons and Analysis

Visual comparisons between real and generated galaxy images further illustrate the model's ability to capture the morphological characteristics associated with different redshifts. Figure 6 presents side-by-side images of real galaxies and DDPM-generated galaxies conditioned on the same redshifts. The generated images exhibit realistic galaxy features, capturing variations in structure, size, and brightness distribution that are consistent with changes in redshift. Caution: The RGB images of the galaxies presented in this paper uses (g,r,i) to make the false color image as recommnended in Li et al. [2024b]. Consequently, the i and r channels can pick up heat and dust and project it in the image, making the image appear noise. As a consequence, some of the DDPM generated images will also have this as an artifact in when projecting the output to a False color.

As redshift increases, galaxies tend to appear smaller and less defined due to cosmological effects such as cosmic expansion and the redshifting of light. Our model reflects these trends, indicating that it has learned meaningful relationships between redshift and galaxy morphology, despite only being conditioned on redshift and not explicitly provided with morphological labels during training.

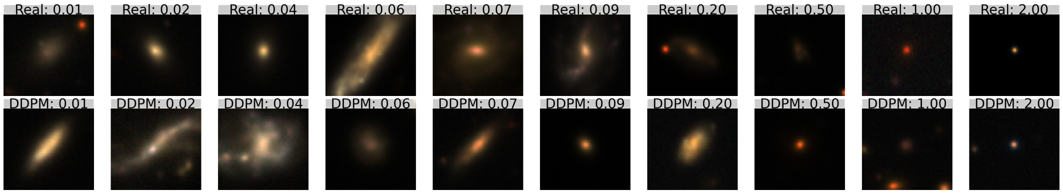

Figure 6: Visual comparison of real and synthesized galaxies across redshifts. (Top row) Examples of real galaxies from the Hyper Suprime-Cam test set at various spectroscopic redshifts. (Bottom row) DDPM-generated galaxies conditioned on the same respective redshifts as the real examples above them. The model successfully captures redshift-dependent visual characteristics, including changes in apparent size, color, and structural definition.

These results suggest that our model not only generates visually plausible galaxy images but also accurately reflects the underlying physical properties associated with different redshifts. The ability of the DDPM to implicitly capture galaxy morphology demonstrates the effectiveness of continuous conditioning in modeling complex, continuous variations in data, such as galaxy evolution over cosmic time.

5 Discussion and Limitations

Despite the promising results of our model, several limitations need to be acknowledged. One of the key challenges is that galaxies do not evolve in isolation. Our model currently treats each galaxy independently, failing to account for the complex interactions between galaxies and their environments, such as mergers or gravitational interactions. These interactions play a significant role in galaxy evolution, and ignoring them may limit the physical when applying it to clusters of galaxies.

Additionally, while our model successfully generates realistic galaxy images conditioned on redshift, the denoising process might inadvertently remove noise that encodes important physical information in later stages of galaxy evolution. This smoothing effect could reduce the overall astrophysical validity of the generated data, particularly when simulating high-redshift galaxies. Additionally metrics such as Sérsic index, ellipticity, and isophotal area can potentially have higher variance when perturbing the redshift too much. To understand this, we took a random sample real images from the test dataset. On the left of Fig. 8 is the initial image. Note that same galaxies appear to be noisy, but this is merely dust and residual heat being captured in the image. Since the conditioning of the DDPM was on z with a Gaussian perturbation, we feed the image in the model and denoise it at $z + \Delta z$, where $\Delta z = 0.1$. Notice that same of the galaxies stay mostly the same (with a slightly more red hue towards the end), but row 3 has dramatic changes.

Moreover, the model's performance is notably less reliable at higher redshifts, where the training data is sparse. This limitation indicates that the model struggles to capture the full diversity of galaxy morphologies at these redshifts, leading to increased variability in the generated images and less accurate redshift conditioning. To make matters more challenging, other scientific domains have found that model performance may not capture scientifically relevant structure even in simpler models such as VAE's Lizarraga et al. [2022], Nunez et al. [2021], Lizarraga et al. [2021], VQ-VAE's Lizarraga et al. [2024b], and MLP's Ren et al. [2025], Honig et al. [2025] further amplifying the challenge of correctly interpreting the results of more sophisticaged architectures like a DDPM.

6 Conclusion

In this work, we introduced a novel approach to generating galaxy images using Denoising Diffusion Probabilistic Model (DDPM), conditioned on continuous redshift values. Our results show that the DDPM effectively captures essential physical attributes of galaxies, such as semi-major axis, isophotal area, ellipticity, and Sérsic index, with high fidelity to the true data distribution. This suggests that redshift, a measure of both age and distance, serves as a strong predictor of galaxy structure, even without direct morphological inputs.

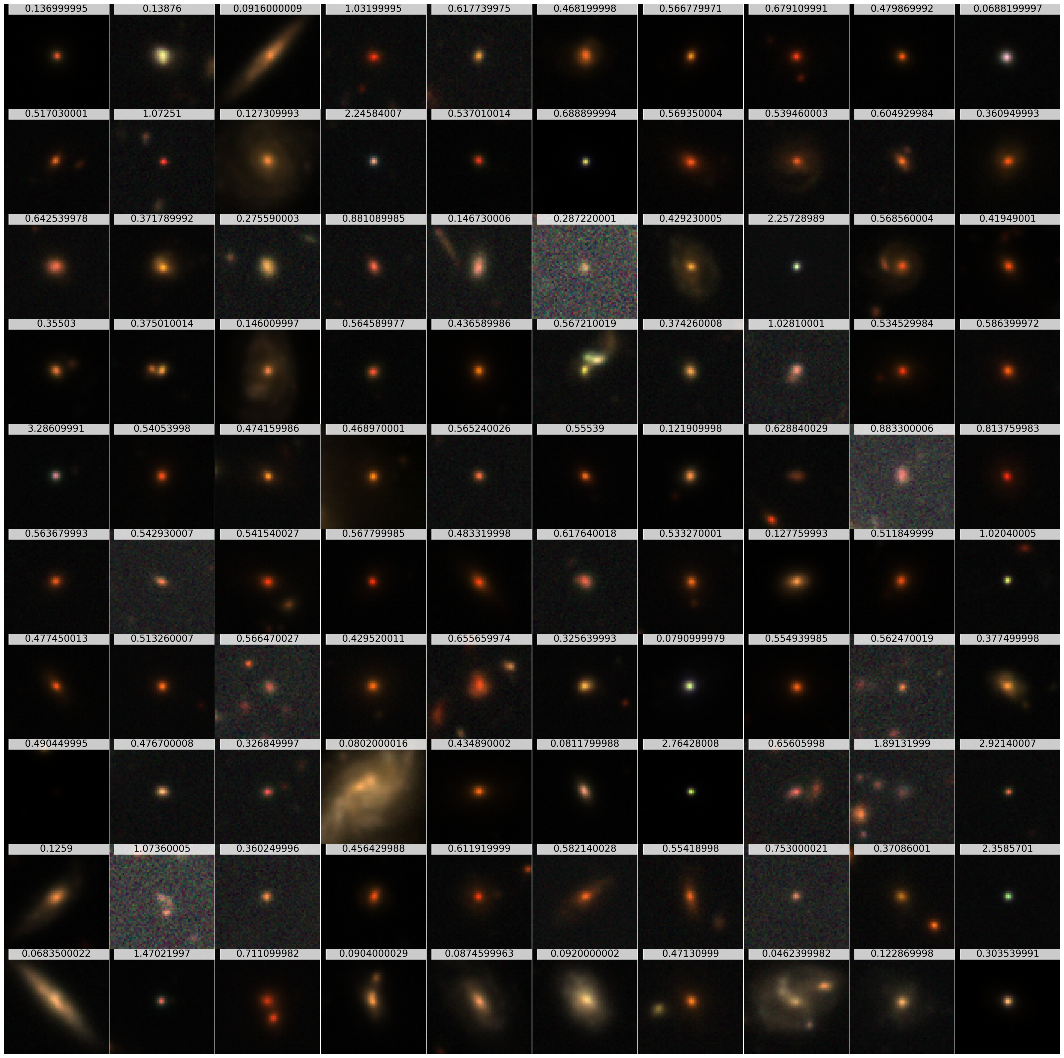

Figure 7: DDPM (False Color) Galaxies Generated at non-cherry-picked redshift values.

Future work should focus on extending this approach toward models that can learn the physical evolution of galaxies more directly. Reproducing the morphological characteristics [e.g., Conselice, 2014a] is the first step to embed the physics of galaxy evolution into an neural network. To demonstrate more direct connection to physics, one should also apply more stringent tests. For example, it's uncertain if models produce galaxies that have the same star formation rate density evolution [e.g., Madau and Dickinson, 2014] or physical changes through galaxy mergers Lotz et al. [2008].

Moreover, considering DDPM's ability to interpolate between modes of the learned probability distribution, we propose raises the question if DDPM's can be utilized for dynamic visualizations of galaxy evolution as a function of redshift. Such a framework could serve as a powerful tool for studying galaxy formation and evolution across cosmic timescales.

6.1 Future Work

There are few auto-regressive (LLM-based) models on galaxy data. One main concern as mentioned earlier the amount of data in survey's such as the HyperCam-Suprime dataset are very low for auto-regressive models. However a new line of LLM models with latent cross-attention mechanisms have been shown to work well with low-data bottle necks and offer interpretability due to the latent-prompt

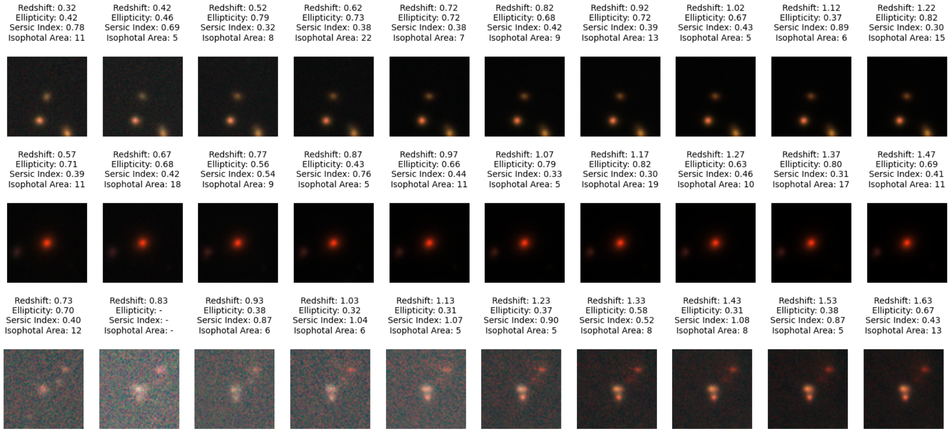

Figure 8: Real images and their corresponding denoised outputs for pertubed $z + \Delta z$. Viewing physical metrics as the we construct a trajectory based on the real image (Left). The model is only conditioned on redshift, while metrics such as Sérsic Index, Ellipticity, Isophotal area may be assocated with certain redshift bins as in Fig. 3, the variance of these metrics can be higher for these trajectories which are out of distribution. Note that depending on noise-to-signal, some metrics computations are not computed and are left blank.

learning the heirarchical structure of the data through a meta-learning process Kong et al. [2024], Lizarraga [2025]. Future work can explore these directions further.

Acknowledgments and Disclosure of Funding

This work was partially supported by CSREx - SOU, NSF DMS-2015577, NSF DMS-2415226, NSF-DGE-2034835 and a gift fund from Amazon.

References

T. M. C. Abbott et al. Dark energy survey year 3 results: Cosmological constraints from galaxy clustering and weak lensing. *Physical Review D*, 105(2):023520, 2022.

C. P. Ahn et al. The ninth data release of the sloan digital sky survey: First spectroscopic data from the sdss-iii baryon oscillation spectroscopic survey. *The Astrophysical Journal Supplement Series*, 203(2):21, 2012.

H. Aihara et al. Second data release of the hyper suprime-cam subaru strategic program. *Publications of the Astronomical Society of Japan*, 71(5):114, 2019.

Martin Arjovsky, Soumith Chintala, and Léon Bottou. Wasserstein gan. In *International Conference on Machine Learning (ICML)*, pages 214–223, 2017.

Christopher J. Conselice. The Evolution of Galaxy Structure Over Cosmic Time. *Annual Review of Astronomy and Astrophysics*, 52(1):291–337, 2014a. doi: 10.1146/annurev-astro-081913-040037.

Christopher J Conselice. The evolution of galaxy structure over cosmic time. *Annual Review of Astronomy and Astrophysics*, 52:291–337, 2014b.

Prafulla Dhariwal and Alexander Nichol. Diffusion Models Beat GANs on Image Synthesis. In M. Ranzato, A. Beygelzimer, Y. Dauphin, P.S. Liang, and J. Wortman Vaughan, editors, *Advances in Neural Information Processing Systems*, volume 34, pages 8780–8794. Curran Associates, Inc., 2021. URL `https://proceedings.neurips.cc/paper_files/paper/2021/file/49ad23d1ec9fa4bd8d77d02681df5cfa-Paper.pdf`.

Xin Ding, Yongwei Wang, Kao Zhang, and Z. Jane Wang. CCDM: Continuous conditional diffusion models for image generation, 2024.

Quynh Do, Andrew Lizarraga, Claudia Yeh, et al. Galaxiesml: A dataset of galaxy images with matched redshifts. *Zenodo*, 2024a. URL `https://zenodo.org/records/11117528`.

Tuan Do, Evan Jones, Bernie Boscoe, Yunqi (Billy) Li, and Kevin Alfaro. GalaxiesML: an imaging and photometric dataset of galaxies for machine learning, June 2024b. URL `https://doi.org/10.5281/zenodo.11117528`.

Patrick Esser, Robin Rombach, and Björn Ommer. Taming transformers for high-resolution image synthesis. *Proceedings of the IEEE/CVF Conference on Computer Vision and Pattern Recognition (CVPR)*, pages 12873–12883, 2021.

Ian J. Goodfellow, Jean Pouget-Abadie, Mehdi Mirza, Bing Xu, David Warde-Farley, Sherjil Ozair, Aaron Courville, and Yoshua Bengio. Generative adversarial nets. In Z. Ghahramani, M. Welling, C. Cortes, N. Lawrence, and K.Q. Weinberger, editors, *Advances in Neural Information Processing Systems*, volume 27. Curran Associates, Inc., 2014. URL `https://proceedings.neurips.cc/paper_files/paper/2014/file/f033ed80deb0234979a61f95710dbe25-Paper.pdf`.

Dan Hendrycks and Kevin Gimpel. Gaussian error linear units (gelus). *arXiv preprint arXiv:1606.08415*, 2016.

Martin Heusel, Hubert Ramsauer, Thomas Unterthiner, Bernhard Nessler, and Sepp Hochreiter. GANs Trained by a Two Time-Scale Update Rule Converge to a Local Nash Equilibrium. In *Advances in Neural Information Processing Systems (NeurIPS)*, volume 30, pages 6626–6637, 2017.

Makoto Ando Hiroaki Aihara, Yusra AlSayyad and et al. Second data release of the Hyper Suprime-Cam Subaru Strategic Program. *Publications of the Astronomical Society of Japan*, 71(6):114, 10 2019. ISSN 0004-6264. doi: 10.1093/pasj/psz103. URL `https://doi.org/10.1093/pasj/psz103`.

Jonathan Ho, Ajay Jain, and Pieter Abbeel. Denoising Diffusion Probabilistic Models. In H. Larochelle, M. Ranzato, R. Hadsell, M.F. Balcan, and H. Lin, editors, *Advances in Neural Information Processing Systems*, volume 33, pages 6840–6851. Curran Associates, Inc., 2020a. URL `https://proceedings.neurips.cc/paper_files/paper/2020/file/4c5bcfec8584af0d967f1ab10179ca4b-Paper.pdf`.

Jonathan Ho, Ajay Jain, and Pieter Abbeel. Denoising diffusion probabilistic models. In *Advances in Neural Information Processing Systems (NeurIPS)*, pages 6840–6851, 2020b.

Edouardo Honig, Andrew Lizarraga, Zijun Frank Zhang, and Ying Nian Wu. Better prompt compression without multi-layer perceptrons, 2025. URL `https://arxiv.org/abs/2501.06730`.

Eric Hanchen Jiang, Yasi Zhang, Zhi Zhang, Yixin Wan, Andrew Lizarraga, Shufan Li, and Ying Nian Wu. Unlocking the potential of text-to-image diffusion with pac-bayesian theory, 2024. URL `https://arxiv.org/abs/2411.17472`.

Tero Karras, Miika Aittala, Jaakko Lehtinen, Janne Hellsten, Timo Aila, and Samuli Laine. Analyzing and Improving the Training Dynamics of Diffusion Models. In *Proc. CVPR*, 2024.

Diederik P Kingma and Max Welling. Auto-encoding variational bayes. In *International Conference on Learning Representations (ICLR)*, 2014.

Deqian Kong, Dehong Xu, Minglu Zhao, Bo Pang, Jianwen Xie, Andrew Lizarraga, Yuhao Huang, Sirui Xie, and Ying Nian Wu. Latent plan transformer for trajectory abstraction: Planning as latent space inference. In A. Globerson, L. Mackey, D. Belgrave, A. Fan, U. Paquet, J. Tomczak, and C. Zhang, editors, *Advances in Neural Information Processing Systems*, volume 37, pages 123379–123401. Curran Associates, Inc., 2024. URL `https://proceedings.neurips.cc/paper_files/paper/2024/file/df22a19686a558e74f038e6277a51f68-Paper-Conference.pdf`.

K. Kuijken et al. The fourth data release of the kilo-degree survey. *Astronomy & Astrophysics*, 625: A2, 2019.

François Lanusse, Rachel Mandelbaum, Siamak Ravanbakhsh, Chun-Liang Li, Peter Freeman, and Barnabás Póczos. Deep generative models for galaxy image simulations. *Monthly Notices of the Royal Astronomical Society*, 504(4):5543–5555, 05 2021. ISSN 0035-8711. doi: 10.1093/mnras/stab1214. URL https://doi.org/10.1093/mnras/stab1214.

E. Lastufka, M. Drozdova, V. Kinakh, D. Piras, and S. Voloshynovskyy. Vision foundation models: can they be applied to astrophysics data?, 2024. URL https://arxiv.org/abs/2409.11175.

Minzhe Li, Andrew Lizarraga, et al. Unredshift: A benchmark for learning galaxy morphology across cosmic time. *arXiv preprint arXiv:2401.12345*, 2024a.

Yun Qi Li, Tuan Do, Evan Jones, Bernie Boscoe, Kevin Alfaro, and Zooey Nguyen. Using Galaxy Evolution as Source of Physics-Based Ground Truth for Generative Models, 2024b. URL https://arxiv.org/abs/2407.07229.

Andrew Lizarraga. Rl isn't enough. *https://drewrl3v.github.io/*, April 2025. URL https://drewrl3v.github.io/blogs/april2025.html.

Andrew Lizarraga, David Lee, Antoni Kubicki, Ashish Sahib, Elvis Nunez, Katherine Narr, and Shantanu H. Joshi. Alignment of tractography streamlines using deformation transfer via parallel transport. In Suheyla Cetin-Karayumak, Daan Christiaens, Matteo Figini, Pamela Guevara, Noemi Gyori, Vishwesh Nath, and Tomasz Pieciak, editors, *Computational Diffusion MRI*, pages 96–105, Cham, 2021. Springer International Publishing. ISBN 978-3-030-87615-9.

Andrew Lizarraga, Katherine L. Narr, Kirsten A. Donals, and Shantanu H. Joshi. Streamnet: A wae for white matter streamline analysis. In Erik Bekkers, Jelmer M. Wolterink, and Angelica Aviles-Rivero, editors, *Proceedings of the First International Workshop on Geometric Deep Learning in Medical Image Analysis*, volume 194 of *Proceedings of Machine Learning Research*, pages 172–182. PMLR, 18 Nov 2022. URL https://proceedings.mlr.press/v194/lizarraga22a.html.

Andrew Lizarraga, Eric Hanchen Jiang, Jacob Nowack, Yun Qi Li, Ying Nian Wu, Bernie Boscoe, and Tuan Do. Learning the evolution of physical structure of galaxies via diffusion models, 2024a. URL https://arxiv.org/abs/2411.18440.

Andrew Lizarraga, Brandon Taraku, Edouardo Honig, Ying Nian Wu, and Shantanu H. Joshi. Differentiable vq-vae's for robust white matter streamline encodings. In *2024 IEEE International Symposium on Biomedical Imaging (ISBI)*, pages 1–5, 2024b. doi: 10.1109/ISBI56570.2024.10635543.

Ilya Loshchilov and Frank Hutter. Decoupled weight decay regularization. *International Conference on Learning Representations (ICLR)*, 2020.

Jennifer M. Lotz, Patrik Jonsson, T. J. Cox, and Joel R. Primack. Galaxy merger morphologies and time-scales from simulations of equal-mass gas-rich disc mergers. *Monthly Notices of the Royal Astronomical Society*, 391:1137–1162, December 2008. ISSN 0035-8711. doi: 10.1111/j.1365-2966.2008.14004.x.

Piero Madau and Mark Dickinson. Cosmic Star-Formation History. *Annual Review of Astronomy and Astrophysics*, 52:415–486, August 2014. ISSN 0066-4146. doi: 10.1146/annurev-astro-081811-125615.

Berta Margalef-Bentabol, Marc Huertas-Company, Tom Charnock, Carla Margalef-Bentabol, Mariangela Bernardi, Yohan Dubois, Kate Storey-Fisher, and Lorenzo Zanisi. Detecting outliers in astronomical images with deep generative networks. *Monthly Notices of the Royal Astronomical Society*, 496(2):2346–2361, 06 2020. ISSN 0035-8711. doi: 10.1093/mnras/staa1647. URL https://doi.org/10.1093/mnras/staa1647.

Tri Nguyen, Francisco Villaescusa-Navarro, Siddharth Mishra-Sharma, Carolina Cuesta-Lazaro, Paul Torrey, Arya Farahi, Alex M. Garcia, Jonah C. Rose, Stephanie O'Neil, Mark Vogelsberger, Xuejian Shen, Cian Roche, Daniel Anglés-Alcázar, Nitya Kallivayalil, Julian B. Muñoz, Francis-Yan Cyr-Racine, Sandip Roy, Lina Necib, and Kassidy E. Kollmann. How dreams are made: Emulating satellite galaxy and subhalo populations with diffusion models and point clouds, 2024. URL https://arxiv.org/abs/2409.02980.

Alexander Quinn Nichol and Prafulla Dhariwal. Improved denoising diffusion probabilistic models. *arXiv preprint arXiv:2102.09672*, 2021.

Atsushi J. Nishizawa, Bau-Ching Hsieh, Masayuki Tanaka, and Tadafumi Takata. Photometric Redshifts for the Hyper Suprime-Cam Subaru Strategic Program Data Release 2, 2020. URL `https://arxiv.org/abs/2003.01511`.

Elvis Nunez, Andrew Lizarraga, and Shantanu H. Joshi. Srvfnet: A generative network for unsupervised multiple diffeomorphic functional alignment. In *Proceedings of the IEEE/CVF Conference on Computer Vision and Pattern Recognition (CVPR) Workshops*, pages 4481–4489, June 2021.

Jie Ren, Xinhao Zheng, Jiyu Liu, Andrew Lizarraga, Ying Nian Wu, Liang Lin, and Quanshi Zhang. Monitoring primitive interactions during the training of dnns. *Proceedings of the AAAI Conference on Artificial Intelligence*, 39(19):20183–20191, Apr. 2025. doi: 10.1609/aaai.v39i19.34223. URL `https://ojs.aaai.org/index.php/AAAI/article/view/34223`.

Michael J Smith, James E Geach, Ryan A Jackson, Nikhil Arora, Connor Stone, and Stéphane Courteau. Realistic galaxy image simulation via score-based generative models. *Monthly Notices of the Royal Astronomical Society*, 511(2):1808–1818, 01 2022. ISSN 0035-8711. doi: 10.1093/mnras/stac130. URL `https://doi.org/10.1093/mnras/stac130`.

Jascha Sohl-Dickstein, Eric Weiss, Niru Maheswaranathan, and Surya Ganguli. Deep unsupervised learning using nonequilibrium thermodynamics. In Francis Bach and David Blei, editors, *Proceedings of the 32nd International Conference on Machine Learning*, volume 37 of *Proceedings of Machine Learning Research*, pages 2256–2265, Lille, France, 07–09 Jul 2015a. PMLR. URL `https://proceedings.mlr.press/v37/sohl-dickstein15.html`.

Jascha Sohl-Dickstein, Eric A. Weiss, Niru Maheswaranathan, and Surya Ganguli. Deep unsupervised learning using nonequilibrium thermodynamics. In *Proceedings of the 32nd International Conference on International Conference on Machine Learning - Volume 37*, ICML'15, page 2256–2265. JMLR.org, 2015b.

Jiaming Song, Chenlin Meng, and Stefano Ermon. Denoising Diffusion Implicit Models. *ArXiv*, abs/2010.02502, 2020. URL `https://api.semanticscholar.org/CorpusID:222140788`.

Zhiwei Xue, Yuhang Li, Yash J. Patel, and Jeffrey Regier. Diffusion Models for Probabilistic Deconvolution of Galaxy Images. *ArXiv*, abs/2307.11122, 2023. URL `https://api.semanticscholar.org/CorpusID:260091385`.

Yaxuan Zhu, Zehao Dou, Haoxin Zheng, Yasi Zhang, Ying Nian Wu, and Ruiqi Gao. Think twice before you act: Improving inverse problem solving with mcmc, 2024. URL `https://arxiv.org/abs/2409.08551`.

A Appendix

A.1 Architecture and Training Details

The UNet model is employed as the backbone for the denoising process in the DDPM. The model is conditioned on the time step t and the redshift z. The detailed layer configuration for the UNet is provided in Table 2.

Layer	Input Channels	Output Channels	Other Parameters
DoubleConv (Initial)	5	64	Kernel: 3x3, Padding: 1, Activation: GELU, GroupNorm
Down1	64	128	Embedding Dim: 256, MaxPool: 2x2, Residual: True
Down2	128	256	Embedding Dim: 256, MaxPool: 2x2, Residual: True
Down3	256	256	Embedding Dim: 256, MaxPool: 2x2, Residual: True
Bottleneck 1	256	512	Kernel: 3x3, Padding: 1, Activation: GELU, GroupNorm
Bottleneck 2	512	512	Kernel: 3x3, Padding: 1, Activation: GELU, GroupNorm
Bottleneck 3	512	256	Kernel: 3x3, Padding: 1, Activation: GELU, GroupNorm
Up1	512	128	Embedding Dim: 256, Upsample: 2x2, Residual: True
Up2	256	64	Embedding Dim: 256, Upsample: 2x2, Residual: True
Up3	128	64	Embedding Dim: 256, Upsample: 2x2, Residual: True
Output Conv	64	5	Kernel: 1x1

Table 2: UNet Layer Configuration

The DDPM processes these $64 \times 64 \times 5$ channel galaxy images. The $T = 1000$ diffusion timesteps, with noise variances β_t following the linear schedule from $\beta_1 = 10^{-4}$ to $\beta_T = 0.02$, dictate the gradual introduction of noise in the forward process (Equation 1). The model is trained by minimizing the Huber loss between the true noise ϵ and the network's prediction $\epsilon_\theta(x_t, t, \tilde{z})$. The AdamW optimizer, with the specified learning rate and gradient clipping, ensures stable training. The EMA of model parameters (decay rate $\beta_{\text{EMA}} = 0.995$, starting after 2000 steps) further contributes to robust generation quality [Karras et al., 2024].